THE JOURNAL OF BIOLOGICAL CHEMISTRY VOL. 284, NO. 27, pp. 18471–18480, July 3, 2009
Printed in the U.S.A.

WNK4 Diverts the Thiazide-sensitive NaCl Cotransporter to the Lysosome and Stimulates AP-3 Interaction*

Received for publication, February 24, 2009, and in revised form, April 14, 2009 Published, JBC Papers in Press, April 28, 2009, DOI 10.1074/jbc.M109.008185

Arohan R. Subramanya[‡§¶1], **Jie Liu**[‡], **David H. Ellison**[‖], **James B. Wade**[‡], **and Paul A. Welling**[‡]

From the Departments of [‡]*Physiology and* [§]*Medicine, University of Maryland School of Medicine, and the* [¶]*Department of Veterans Affairs Medical Center, Baltimore, Maryland 21201 and the* [‖]*Division of Nephrology and Hypertension, Oregon Health and Science University, Portland, Oregon 97239*

With-no-lysine kinase 4 (WNK4) inhibits electroneutral sodium chloride reabsorption by attenuating the cell surface expression of the thiazide-sensitive NaCl cotransporter (NCC). The underlying mechanism for this effect remains poorly understood. Here, we explore how WNK4 affects the trafficking of NCC through its interactions with intracellular sorting machinery. An analysis of NCC cell surface lifetime showed that WNK4 did not alter the net rate of cotransporter internalization. In contrast, direct measurements of forward trafficking revealed that WNK4 attenuated the rate of NCC surface delivery, inhibiting the anterograde movement of cotransporters traveling to the plasma membrane from the trans-Golgi network. The response was paralleled by a dramatic reduction in NCC protein abundance, an effect that was sensitive to the lysosomal protease inhibitor leupeptin, insensitive to proteasome inhibition, and attenuated by endogenous WNK4 knockdown. Subcellular localization studies performed in the presence of leupeptin revealed that WNK4 enhanced the accumulation of NCC in lysosomes. Moreover, NCC immunoprecipitated with endogenous AP-3 complexes, and WNK4 increased the fraction of cotransporters that associate with this adaptor, which facilitates cargo transport to lysosomes. WNK4 expression also increased LAMP-2-positive lysosomal content, indicating that the kinase may act by a general AP-3-dependent mechanism to promote cargo delivery into the lysosomal pathway. Taken together, these findings indicate that WNK4 inhibits NCC activity by diverting the cotransporter to the lysosome for degradation by way of an AP-3 transport carrier.

The with-no-Lysine (WNK)[2] kinases are a unique family of serine-threonine protein kinases that regulate ion transport in diverse epithelia (1). In the kidney the gene products of several members of the WNK family, including WNK1, WNK3, and WNK4, converge in a signaling network that coordinates distal nephron sodium chloride and potassium handling. WNK4 participates in this network by suppressing NaCl reabsorption via the thiazide-sensitive NaCl cotransporter (NCC, SLC12A3), and potassium secretion via the potassium channel Kir 1.1 (ROMK) (2, 3). The importance of this signaling pathway is underscored by a link to human disease; *WNK4* mutations cause familial hyperkalemic hypertension (pseudohypoaldosteronism type II, Gordon's syndrome), an autosomal dominant disorder featuring chloride-dependent thiazide-sensitive hypertension and hyperkalemia (4). These mutations release NCC from inhibition, leading to an increase in renal sodium chloride reabsorption and blood pressure (2, 5).

Ample evidence demonstrates that WNK4 suppresses NCC activity, at least in part by modulating its cell surface expression. This effect has been observed at steady state in multiple heterologous overexpression systems, including *Xenopus* oocytes (2, 5, 6), COS-7 cells (7), and polarized Madin-Darby canine kidney cells epithelia (8). More recently, the inhibitory effect of wild type WNK4 on NCC has been verified *in vivo*. Mice overexpressing wild type WNK4 exhibit a reduced total amount of NCC expressed at the apical surface of the distal convoluted tubule (DCT), coincident with a reduction in DCT cell mass (9). Conversely, knock-in mice bearing a familial hyperkalemic hypertension-causing *WNK4* mutation overexpress NCC at the apical surface, leading to chloride-dependent hypertension and hyperkalemia (10).

Although the underlying mechanism by which WNK4 regulates NCC trafficking remains unresolved, some clues are available. Two groups have shown that, unlike the effect of WNK4 on ROMK channel activity (3), WNK4-mediated NCC inhibition is not attenuated by a dominant-negative dynamin mutant (6, 7). These observations strongly suggest that the kinase acts via independent mechanisms to modulate the cell surface expression of NCC and ROMK. Cai *et al.* (7) found that the suppressive effect of WNK4 on NCC was sensitive to vacuolar H+ ATPase inhibition, suggesting that the kinase might promote the trafficking of NCC to a low pH endosomal compartment. However, the precise identity of this compartment and the mechanism by which the cotransporter arrives there remains undefined.

In this study we elucidated the mechanism by which WNK4 suppresses NCC surface expression by directly measuring the effect of WNK4 on NCC cell surface lifetime, forward trafficking, subcellular localization, and interactions with intracellular

* This work was supported, in whole or in part, by National Institutes of Health Grants DK072865 (to A. R. S.), DK063049 (to P. A. W.), DK054231 (to P. A. W.), and DK051496 (to D. H. E.). This work was also supported by American Heart Association Grant 0755503U (to J. B. W.), a United States Department of Veterans Affairs Mid-Level Career Development Award (to A. R. S.), and a Mini-Grant from the National Kidney Foundation of Maryland (to A. R. S.).

[1] To whom correspondence should be addressed: 660 W. Redwood St., HH517, Baltimore, MD 21201. Tel.: 410-706-2653; Fax: 401-706-8341; E-mail: asubr001@umaryland.edu.

[2] The abbreviations used are: WNK, with-no-lysine; NCC, thiazide-sensitive NaCl cotransporter; ROMK, potassium channel Kir 1.1; TGN, trans-Golgi network; BFA, brefeldin A; HEK, human embryonic kidney; HA, hemagglutinin; siRNA, small interfering RNA; LAMP, lysosome-associated membrane protein; FBS, fetal bovine serum; PBS, phosphate-buffered saline.

trafficking machinery. Our results show that WNK4 does not affect the net internalization rate of NCC expressed at the cell surface. Instead, WNK4 influences the biosynthetic trafficking of NCC, diverting itinerant cotransporters exiting the trans-Golgi network (TGN) away from the plasma membrane and to the lysosome for degradation. Consistent with this observation, WNK4 enhances the physical association between NCC and the AP-3 adaptor complex, which marks cargo for sorting to lysosomes. Thus, these findings reveal a novel mechanism by which cotransporters destined for the cell surface are instead bypassed directly into the endolysosomal pathway for degradation.

EXPERIMENTAL PROCEDURES

Molecular Biology—Previously described mouse NCC and mouse WNK4 clones were used for these studies. For *Xenopus laevis* oocyte experiments, NCC (11) and WNK4-(168–1222) (12, 13) were subcloned into the expression vector pgh19. For forward trafficking studies in mammalian cells, NCC was subcloned to pcDNA3.1 (Invitrogen), and an amino-terminal hemagglutinin epitope was generated via a PCR-based strategy. 2×HA-NCC, an NCC construct containing a double hemagglutinin epitope in the second extracellular loop of the cotransporter, was generated by using a PCR-based strategy to introduce the epitope in-frame and upstream of the NCC AccI site in pgh19. The tagged construct was subsequently subcloned to the EcoRI site of pcDNA3.1 for studies in mammalian cells. Full-length mouse WNK4 (2) was subcloned from pgh19 to pMO-Myc (gift of David Pearce, University of California at San Francisco). All cDNA sequences were confirmed by dye termination sequencing (University of Maryland Biopolymer Core Facility).

Antibodies and Reagents—The following commercial antibodies were used: mouse monoclonal anti-HA (HA-11, Covance), rat monoclonal anti-HA high affinity (3F10, Roche Applied Science), rabbit polyclonal anti-c-Myc (Santa Cruz), rabbit polyclonal anti-human WNK4 (Novus Biologicals), mouse monoclonal anti LAMP-2 (H4B4 supernatant, Developmental Studies Hybridoma Bank, University of Iowa), rabbit polyclonal anti-tubulin (Sigma), mouse monoclonal anti-δ-adaptin (BD Transduction Laboratories), Alexa Fluor-488 anti-rat, 568 anti-mouse, and 633 anti-rabbit (Invitrogen/Molecular Probes), fluorescein isothiocyanate anti-rat and Cy3 anti-rabbit (Zymed Laboratories Inc.); horseradish peroxidase-conjugated goat anti-mouse and goat anti-rabbit antibodies (Jackson ImmunoResearch). Affinity-purified polyclonal rabbit anti-mouse NCC antibody, which recognizes the cytoplasmic amino terminus of the cotransporter, was described previously (14). Leupeptin and MG-132 were obtained from Sigma.

NCC Activity Measurements—Linearization of the NCC and WNK4-(168–1222) plasmid constructs, *in vitro* transcription of the linear templates, harvesting of stage V-VI oocytes from *X. laevis* frogs, cRNA injection, and steady state ^{22}Na uptake experiments were carried out essentially as described previously (2). For the dynamic cell surface lifetime assay, injected oocytes were placed in chloride-free ND96 medium 4 days post-injection and 24 h before the first uptake measurement. At the start of the time course, all experimental groups except for the zero and 1-h time points were moved to chloride-free ND96 containing 10 μM brefeldin A (BFA, Sigma). Thirty minutes before the addition of uptake medium, oocytes were switched to chloride-free ND96 containing transport inhibitors (1 mM ouabain, 100 μM amiloride, and 100 μM bumetanide, Sigma); again, all experimental groups were incubated in BFA except for the zero and 1-h time points. The oocytes were then transferred to isotonic uptake medium containing 10μCi/ml $^{22}Na^+$ with transport inhibitors and incubated at 30 °C for 1 h. For these incubations all experimental groups were subjected to BFA-containing isotonic uptake medium, with the exception of the time 0 measurement, which was incubated in BFA-free uptake medium. All experimental groups were washed 3 times in ice-cold BFA-containing isotonic uptake medium. Cells were then lysed, and counts were measured using previously described methods (11). For the forward trafficking assay, oocytes were incubated in 10 μM BFA-containing chloride-free ND96 for 10 h before the first uptake. For time 0, all transport inhibitor-containing solutions and washes were carried out in BFA-containing medium. For all other time points, the BFA-containing chloride-free ND96 was removed with five washes of BFA-free chloride-free ND96, and all subsequent steps were carried out in BFA-free media.

Cell Culture and Transfection—HEK-293H (Invitrogen) and COS-7 (ATCC) cells were cultured in Dulbecco's modified Eagle's medium supplemented with 10% FBS, L-glutamine, and penicillin/streptomycin at 37 °C. Transient transfections were performed using either FuGENE 6 (Roche Applied Science) or Lipofectamine 2000 (Invitrogen) per the manufacturers' recommendations. Stable transfectants of the 2×HA-NCC clone were generated in HEK-293H cells by selection of FuGENE 6-transfected cells with cloning cylinders after incubation in Dulbecco's modified Eagle's medium-containing 500 μg/ml G418 (Invitrogen). Two different clones expressing HA-tagged NCC protein were used for these studies with identical results.

Quantitative Antibody Binding Cell Surface Luminometry—2×HA-NCC cell surface expression was quantified by chemiluminescence using methods similar to those described previously (15). HEK-293H cells were transiently transfected at 90% confluence on 6-well Biocoat plates (BD Biosciences). 48 h post-transfection, cells were washed twice with cold HEPES buffer (25 mM HEPES, 140 mM NaCl, 5.4 mM KCl, 1.8 mM $CaCl_2$, 15 mM glucose, pH 7.4) and fixed on ice for 15 min in 2% paraformaldehyde in HEPES buffer. The cells were washed 3 times, blocked in 5% FBS in HEPES buffer for 30 min, and incubated with HA-11 antibody (1:500 dilution in HEPES buffer with 0.5% FBS) at room temperature for 1 h. The cells were washed 3 times, incubated with an anti-mouse horseradish peroxidase-conjugated secondary antibody (1:1000 dilution in HEPES buffer with 0.5% FBS) for 30 min, washed 3 more times, gently scraped from the plates, and resuspended into 0.5 ml of cold HEPES buffer. 10 μl of cell suspension was incubated with 100 μl of SuperSignal West Pico chemiluminescent substrate (Pierce), and the chemiluminescence signal was quantified using a Sirius luminometer (Berthold Detection Systems). Measurements were performed in triplicate and timed such that the readings were taken exactly 5 min after the cells were placed in contact with the ECL solution.

Preparation of Whole Cell Lysates and Immunoblotting—Yolk-free lysates of *Xenopus* oocytes were prepared, and immunoblots were performed using previously described methods (2, 16). For HEK-293H whole cell lysates, cells were washed twice with PBS, scraped, collected, and pelleted by centrifugation at 1000 × *g* for 5 min. Post-nuclear lysate supernatants were obtained by passing the pellets 20 times through a 27-gauge needle in HEENG buffer (17) (containing 1% Triton X-100, 1 mM phenylmethylsulfonyl fluoride, and 10 μg/ml each of leupeptin, pepstatin A, and antipain), incubating the samples on ice for 15 min, and removing insoluble material by centrifugation at 16,000 × *g* for 5 min. Protein concentrations were determined by the Bradford method (Bio-Rad protein assay kit). For samples subjected to SDS-PAGE, lysates were denatured in Laemmli buffer, heated for 90 °C × 5 min, and separated on 6 or 7.5% polyacrylamide gels. Dot blots and immunoblotting of samples fractionated by SDS-PAGE were performed as described previously (16, 17).

TGN-to-cell Surface Delivery Assay—293H cells were transiently transfected in 6-well Biocoat plates with the indicated cDNA constructs. Cells were assayed 48 h post-transfection. After 2 washes with Ringer's solution (17), biotinylatable residues at the cell surface were blocked with 1.5 mg/ml Sulfo-NHS acetate (Pierce) in Ringer's solution at 4 °C for 1 h. The cells were then washed, switched to complete Dulbecco's modified Eagle's medium/F-12 medium supplemented with 15 mM HEPES, and incubated at 20 degrees for 2 h to block biosynthetic traffic at the level of the TGN (18, 19). Cells were then released from TGN block by transferring them to 37 °C. At the indicated chase times, cells were biotinylated for 1 h at 4 °C with 1 mg/ml Sulfo NHS-SS-Biotin (Pierce) followed by quenching for 30 min with Ringer's solution containing 50 mM Tris HCl, pH 8.0. Samples were washed and lysed as described above, and 150 μg whole cell lysate was incubated with 50 μl NeutrAvidin-agarose resin (Pierce) with end-over-end rotation overnight at 4 C°. The beads were then washed 4 times with PBS containing 0.1% SDS, and samples were eluted in Laemmli buffer at 90° for 5 min and subjected to SDS-PAGE and immunoblotting as described above.

RNA Interference—Two WNK4 siRNA duplexes were used in knockdown studies. One duplex (siRNA sequence 1) targeted base pairs 1554–1578 of human WNK4 (Stealth Select siRNA, Invitrogen). A second duplex (siRNA sequence 2) was validated in a previous knockdown study (20) and targeted base pairs 776–794 of human WNK4 (Dharmacon). Scrambled siRNA was used for a control (Stealth RNAi negative control duplex, Invitrogen). Cells were transfected in 24-well plates with 200 nM siRNA using Lipofectamine 2000, per the manufacturer's recommendations. 48 h after the initial transfection, cells were retransfected with 200 nM concentrations of the same siRNA duplexes. 24 h after the second transfection, cell samples were harvested for lysis and immunoblotting as described above.

Immunoprecipitation—Whole cell lysates of 293-H cells stably expressing the 2×HA-NCC construct were prepared as described above, with the exception that the Triton concentration was reduced to 0.1%. 300 μg of lysate per sample was diluted with HEENG buffer to a total volume of 300 μl and precleared with 30 μl of protein A/G-agarose slurry (Calbiochem) by end-over-end rotation at 4 °C for 2 h. Primary antibody (1 μg) was added to the precleared lysates, and the samples were rotated in fresh 30-μl aliquots of protein A/G beads overnight at 4 °C. Samples were then centrifuged at low speed, and the beads were washed 4 times in 500 μl of cold PBS. Immunoprecipitates were eluted by heating the beads at 90 °C × 5 min in Laemmli buffer, separated by SDS-PAGE, and analyzed by immunoblotting as described above.

Confocal and Epifluorescent Microscopy—To verify extracellular exposure of the HA epitopes in the 2×HA-NCC construct, COS-7 cells transiently expressing either untagged NCC or 2×HA-NCC for 48 h were fixed under conditions that were either nonpermeabilizing (2% paraformaldehyde for 15 min) or permeabilizing (4% paraformaldehyde for 15 min followed by 3 PBS washes and incubation in 0.1% Triton X-100 for 15 min). After three washes in PBS and a 15-min blocking step in 5% FBS, the coverslips were incubated in 3F10 (1:200) and anti-NCC (1:200) antibodies in 0.5% FBS. The coverslips were then washed three times in PBS and labeled with fluorescein isothiocyanate and Cy3-conjugated secondary antibodies (both at 1:100 concentrations in 0.5% FBS). After extensive washing, the coverslips were mounted on glass slides with Vectashield (Vector Laboratories) and visualized under epifluorescence using a Zeiss Axiophot microscope.

293-H Cells stably expressing 2×HA-NCC, dispersed in 6-well plates containing Biocoat coverslips (BD Biosciences), were transiently transfected with either pMOmyc-WNK4 or empty pMO-Myc vector. 48 h later, cells were fixed in 4% paraformaldehyde, permeabilized, and blocked as described previously (15). Cells were then incubated with 3F10 (1:200), Myc (1:200), and LAMP-2 (1:30) antibodies in 5% FBS for 1 h at room temperature, washed 3 times in PBS, and incubated with Alexa 488, 568, and 635-conjugated secondary antibodies (all at 1:100 concentration in 0.5% FBS) for 30 min. The coverslips were then washed and mounted as described above, and cells were visualized using a Zeiss 510 confocal microscope.

Data Analysis—For quantification of Western blots, densitometry was carried out with NIH Image software. Improvision Volocity 4 was used for quantification of confocal images. GraphPad Prism software was used for statistical analyses. Comparisons between the two groups were determined by Student's *t* test. Multiple group comparisons were carried out by one-way analysis of variance followed by either Bonferroni's or Dunnett's post hoc tests. A p value of <0.05 was considered significant.

RESULTS

WNK4 Suppresses NCC Forward Trafficking without Affecting Its Rate of Internalization—In principle, WNK4 could influence the plasma membrane expression of NCC by increasing its rate of internalization or attenuating its rate of cell surface arrival from an intracellular compartment. NCC internalization could potentially occur via a number of mechanisms, including dynamin-dependent or independent vesicle-mediated endocytosis, phagocytosis, or macropinocytosis. To determine the effect of WNK4 on these various pathways of entry into the cell, we measured the cell surface lifetime of NCC on the plasma membrane. In these studies, *X. laevis* oocytes were

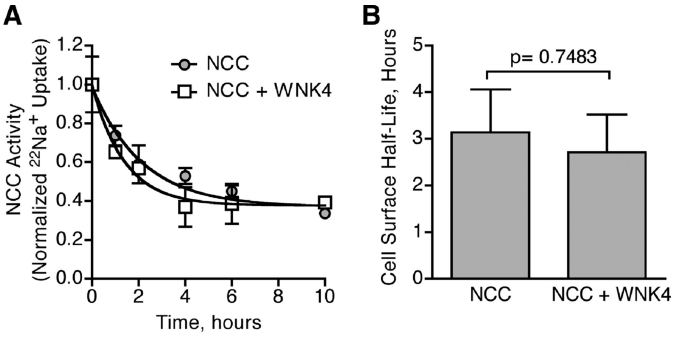

FIGURE 1. **WNK4 does not affect the rate of NCC retrieval from the plasma membrane.** *A*, decay in thiazide-sensitive $^{22}Na^+$ transport, measured in NCC-expressing *X. laevis* oocytes, assessed in the absence or presence of WNK4-(168–1222), a WNK4 construct that stably suppresses NCC activity (12, 13). Measurements were taken after NCC was maximally expressed at the cell surface (4 days post-injection), and oocytes were placed in medium containing 10μM BFA. Each data point represents the mean $^{22}Na^+$ uptake per oocyte ± S.E., normalized to $t = 0$. For each time point $^{22}Na^+$ fluxes were measured in 80–120 oocytes from 4 frogs across 4 separate experiments. *B*, cell surface half-lives of NCC expressed in the absence or presence of WNK4 during BFA incubation, derived from the data shown in *A*. p value = 0.7483 by Student's *t* test.

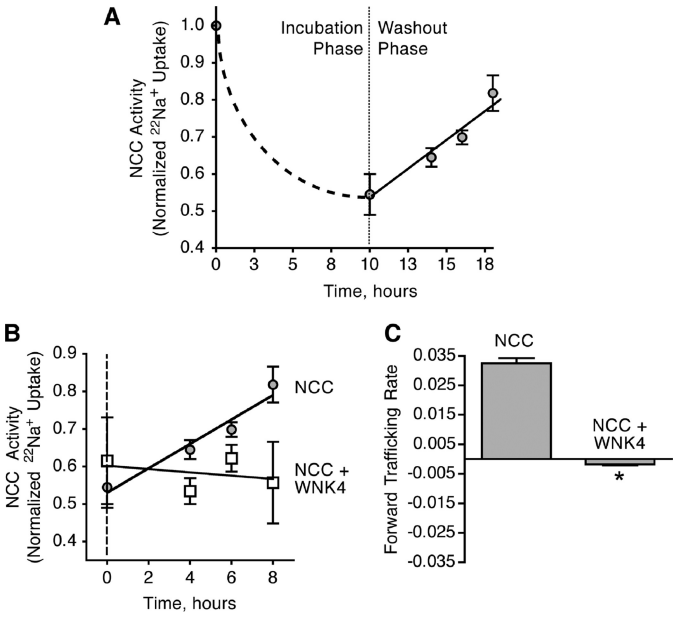

FIGURE 2. **WNK4 inhibits NCC cell surface delivery in *X. laevis* oocytes.** *A*, effect of BFA washout on $^{22}Na^+$ transport, measured in NCC-expressing oocytes preincubated in medium containing 10 μM BFA for 10 h. Measurements were taken 4 days post-injection. Data were normalized to NCC activity at $t = 0$. The *dashed line* is based on data from Fig. 1*A*. *B*, time course of $^{22}Na^+$ transport in oocytes expressing NCC in the absence or presence of WNK4-(168–1222) during the first 8 h after BFA washout. For *panels A* and *B*, each data point represents the mean $^{22}Na^+$ uptake per oocyte ± S.E., normalized to $t = 0$. For each time point, $^{22}Na^+$ fluxes were measured in 50–70 oocytes from 2 frogs across 2 separate experiments. *C*, forward trafficking rate of NCC expressed in the absence or presence of WNK4 during the BFA washout phase, derived from the slopes of the data shown in *B*. *, $p = 0.005$ by Student's *t* test.

injected with cRNAs encoding NCC alone or NCC with WNK4. After a sufficient period of time to allow for maximal NCC cell surface expression (4 days), we monitored the decay in cotransporter activity after the arrival of new cotransporters was blocked with 10 μM BFA. Because BFA selectively and reversibly inhibits the delivery of proteins from the biosynthetic pathway to the cell surface (16, 21–23), the decay in NCC activity corresponds to the net removal of cotransporters from the plasma membrane. The decay curves for oocytes expressing NCC alone *versus* those expressing NCC with WNK4 were indistinguishable (Fig. 1*A*), and regression analysis showed that the two curves were fit by time courses whose half-lives were statistically indistinguishable from one another (Fig. 1*B*). Thus, these results indicate that WNK4 does not alter that net rate of NCC internalization, suggesting that the kinase may instead influence the forward trafficking of the cotransporter.

To test the hypothesis that WNK4 alters the cell surface expression of NCC by suppressing its forward trafficking, we measured the rate of cell surface delivery of the cotransporter. In these studies, *X. laevis* oocytes expressing NCC in the absence or presence of WNK4 for 4 days were treated with 10 μM BFA for an incubation period of 10 h to allow for cotransporters residing at the plasma membrane to be cleared from the surface by internalization. After this incubation period, the BFA was washed out of the oocyte medium, and a gradual recovery of cotransporter activity was observed over the ensuing 8 h (Fig. 2*A*). Because BFA has a selective but reversible inhibitory effect on anterograde trafficking, the recovery in NCC activity during the washout phase must reflect the arrival of cotransporters to the cell surface from an intracellular location. When we compared the washout curves for oocytes expressing NCC to those expressing NCC with WNK4, we found that the recovery of cotransporter activity was substantially blunted in the presence of the kinase (Fig. 2*B*). Accordingly, the slopes of the washout curves, *i.e.* the forward trafficking rate of NCC from its intracellular locations to the cell surface, were statistically different from one another ($p = 0.005$, Fig. 2*C*). These data suggest that WNK4 suppresses the delivery of NCC to the plasma membrane.

To verify and extend these results, we tested whether WNK4 affects the forward trafficking of NCC from within the biosynthetic pathway by directly measuring the time course of NCC delivery to the plasma membrane from the TGN. In this forward trafficking assay, HEK 293H cells transiently expressing amino-terminal HA-tagged NCC were first labeled with Sulfo-NHS acetate. This membrane-impermeant compound covalently attaches an acetyl group to any primary amines that are exposed at the cell surface, rendering surface expressed proteins inaccessible to biotinlyation (24, 25). After Sulfo-NHS Acetate pretreatment, the delivery of unacetylated proteins moving from intracellular compartments to the plasma membrane was quantitatively measured by biotinylating the cell surface at subsequent time points. We confirmed that Sulfo-NHS acetate pretreatment efficiently blocked NCC surface biotinylation in a concentration-dependent manner by performing both treatments in NCC-expressing cells acclimated at 4 °C to arrest protein trafficking. As shown in Fig. 3*A*, pretreatment with 1.5 mg/ml of Sulfo-NHS acetate compound maximally blocked NCC biotinlyation. To measure the surface delivery of cotransporters traveling directly from the TGN, after surface acetylation, cells were incubated at 20 °C for 2 h, a maneuver that blocks the transport of newly synthesized proteins out of the Golgi complex (18, 19, 26). Cells were then moved to 37 °C to allow for forward trafficking to resume, and surface biotiny-

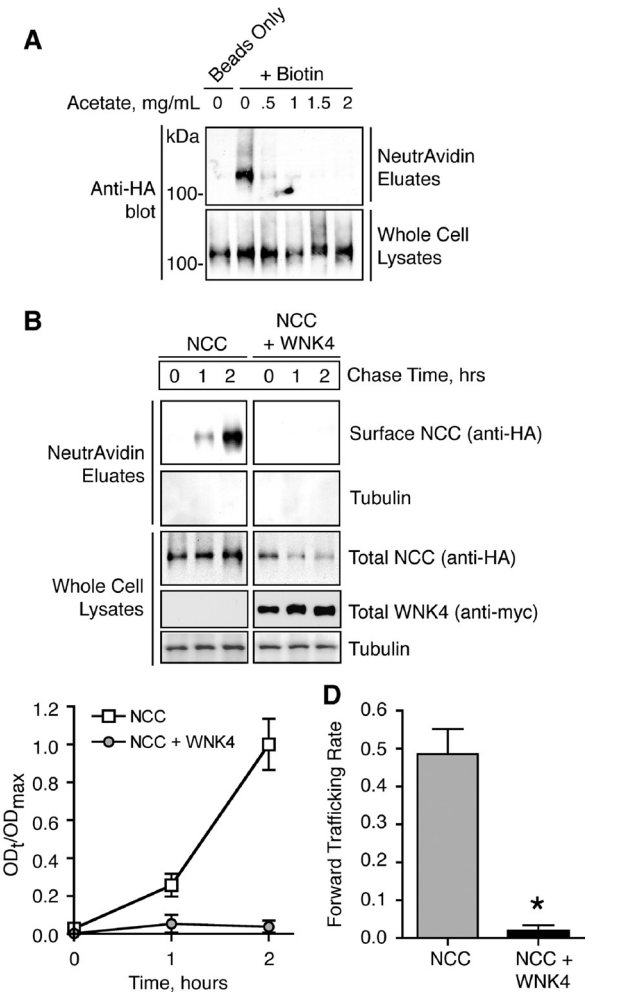

FIGURE 3. **WNK4 inhibits NCC TGN-to-cell surface delivery in HEK-293H cells.** *A*, acetylation of NCC expressed at the plasma membrane blocks cell surface biotinylation. HEK-293H cells were transiently transfected with amino-terminal HA-tagged NCC (HA-NCC) and treated with various concentrations of Sulfo-NHS acetate for 1 h at 4 °C. The acetate compound was then quenched in Tris-containing buffer, and the cells were washed and treated with Sulfo-NHS-SS-Biotin for 1 h at 4 °C. As the concentration of Sulfo-NHS acetate is increased, the amount of surface biotinylated NCC pulled down by the NeutrAvidin-agarose beads decreases. *B*, time course of HA-NCC delivery to the cell surface from the TGN in cells co-expressing either empty vector (*NCC*) or Myc-WNK4 (*NCC + WNK4*). 48 h after transfection cells were pretreated with Sulfo-NHS acetate then placed at 20 °C for 2 h to block biosynthetic traffic at the Golgi. Samples were then warmed to 37 °C and biotinylated at subsequent time points. Western blots of NeutrAvidin eluates and whole cell lysates were performed for HA-NCC and tubulin, an intracellular control. *C*, plot of HA-NCC surface expression, measured by densitometry at various points during the time course (OD_{tz}), normalized to maximum HA-NCC surface expression (at 2 h, OD_{max}). For each experimental group, surface NCC protein abundance was normalized to the whole cell lysate NCC protein densities measured at $t = 0$. Mean ± S.E., $n = 3$. *D*, quantification of the HA-NCC forward trafficking rate, derived as the slopes of the data shown in *C*. *, $p = 0.0024$ by Student's *t* test.

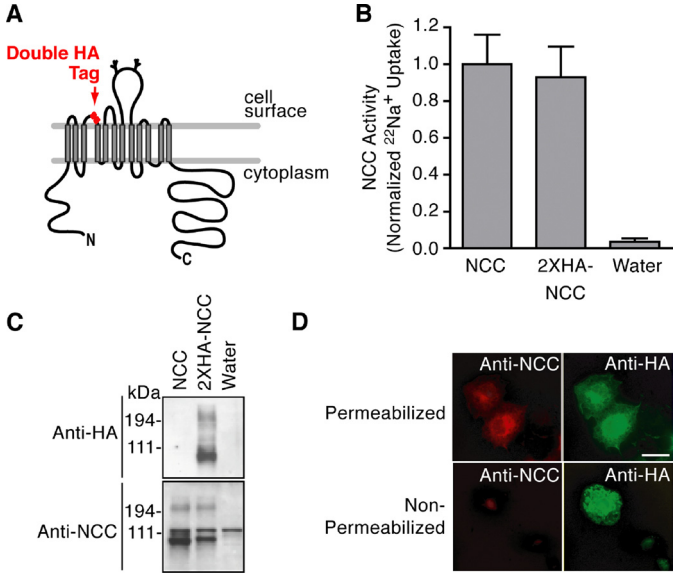

FIGURE 4. **Development of a functional externally tagged cotransporter.** *A*, NCC schematic showing the location of the double hemagglutinin epitope tag. *B*, $^{22}Na^+$ transport measurements of wild type and 2×HA-NCC (mean ± S.E.; fluxes measured in 58–65 oocytes from 2 separate frogs across 3 experiments). *C*, Western blot of whole cell lysates from *Xenopus* oocytes expressing wild type NCC and 2×HA-NCC, using anti-amino-terminal NCC (14) and anti-HA antibodies. *D*, epifluorescence images of immunostained COS-7 cells transiently transfected with wild type NCC or 2×HA-NCC under permeabilized or nonpermeabilized conditions using primary antibodies directed to an intracellular amino-terminal NCC epitope (Cy3/red) or the extracellular HA epitope (fluorescein isothiocyanate/green). Results are representative of three experiments.

lation was performed at multiple time points during the chase period after release from the temperature block. Using this approach, we measured the time course of NCC trafficking to the plasma membrane in the absence or presence of WNK4. In these studies, coexpression of WNK4 with NCC substantially suppressed the amount of NCC delivered to the cell surface within the first 2 h of the forward trafficking time course (Fig. 3, *B* and *C*). Quantification of the forward trafficking rate revealed that WNK4 suppressed the plasma membrane delivery of the cotransporter by nearly 100% (Fig. 3*D*). These findings confirm that WNK4 inhibits the forward trafficking of NCC and specifically demonstrate that WNK4 inhibits the cotransporter delivery rate to the cell surface from the TGN.

WNK4 Inhibits NCC Surface Expression by Promoting Its Lysosomal Routing and Degradation—In these forward trafficking experiments, we noted that the total abundance of NCC appeared to decrease over time when the cotransporter was coexpressed with WNK4 (Fig. 3*B*, *Total NCC* in whole cell lysates). To evaluate this observation in greater detail, we designed an NCC construct that could be used to accurately compare quantitative surface expression to total protein abundance. To this end we engineered an in-frame double hemagglutinin epitope into the putative second extracellular loop of NCC (2×HA-NCC, Fig. 4*A*). We confirmed that this epitope did not alter NCC sodium transport characteristics (Fig. 4*B*). Anti-HA antibodies were highly selective for the tagged construct, and the HA epitope did not significantly alter NCC protein expression (Fig. 4*C*). Finally, the extracellular exposure of the epitope was confirmed by immunofluorescence microscopy. These studies showed that we were able to detect the externally tagged NCC construct with a monoclonal anti-HA antibody under both permeabilized and nonpermeabilized conditions (Fig. 4*D*, *top right* and *bottom right*), whereas a previously described polyclonal antibody directed to an intracellular NCC epitope (14) could only detect the 2×HA-NCC construct under permeabilized conditions (Fig. 4*D*, *top left* and *bottom left*).

Using the 2×HA-NCC construct, we quantified the steady state expression of NCC at the plasma membrane using anti-

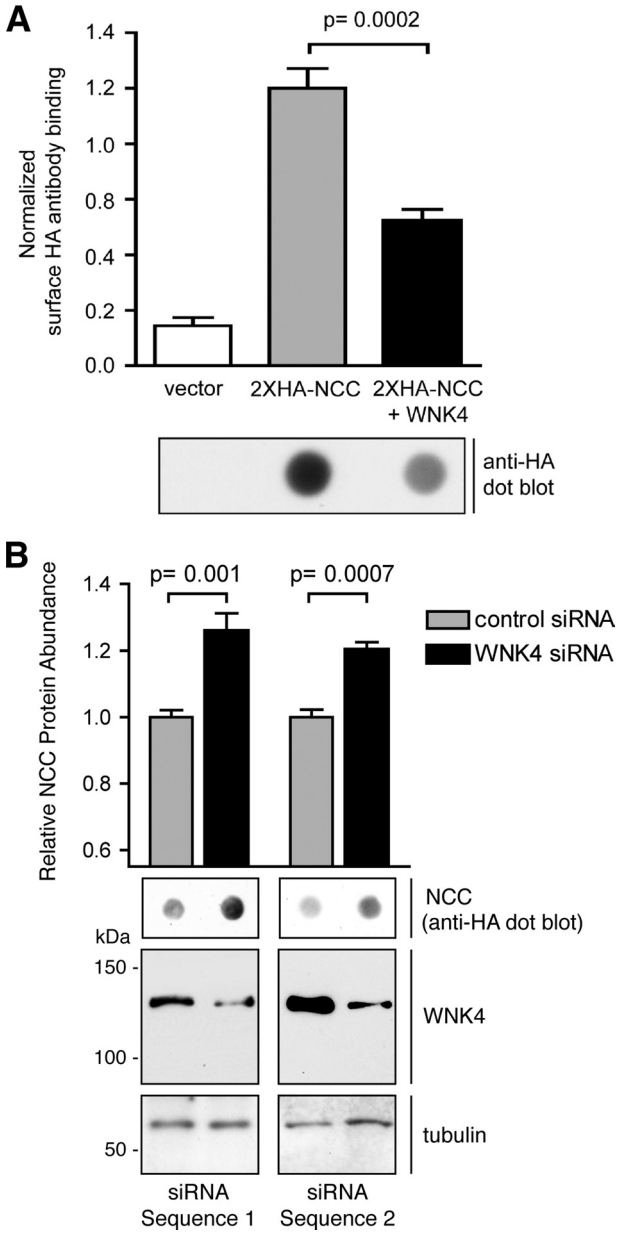

FIGURE 5. **WNK4 decreases steady state NCC surface expression and total protein abundance in HEK-293 cells.** *A*, *top*, quantitative cell surface HA antibody binding and luminometry in cells transiently expressing 1 μg/well empty vector, 0.5 μg/well 2×HA-NCC plus 0.5μg/well empty vector, or 0.5 μg/well 2×HA-NCC plus 0.5μg/well WNK4 (mean ± S.E., $n = 4$). *Bottom*, anti-HA dot blot of whole cell lysates (7 μg of protein) from HEK-293H cells transiently transfected in parallel to the luminometry assays shown in the *top panel*. Representative of four experiments. *B*, HEK-293H cells stably expressing 2×HA-NCC were transiently transfected twice with siRNAs directed against human WNK4 or a control scrambled siRNA, as described under "Experimental Procedures." 24 h after the second transfection cells were harvested, and 4 μg of the whole cell lysates were subjected to immunoblotting. Results are the mean ± S.E., $n = 6$ for *siRNA Sequence 1*, $n = 4$ for *siRNA Sequence 2*.

body binding and cell surface luminometry in HEK 293H cells. Similar to previous studies in other systems (5–8, 13), we found that WNK4 reduced the plasma membrane expression of 2×HA-NCC by 50% (Fig. 5*A*, *top*). Dot blot studies performed in parallel to luminometry measurements demonstrated that the WNK4-mediated decrease in 2×HA-NCC surface expression corresponded with a reduction in total protein abundance (Fig. 5*A*, *bottom*). Thus, in HEK 293H cells, WNK4 overexpression reduces NCC surface expression and total protein abundance.

To determine whether this effect takes place under conditions where the kinase is present at its base-line abundance levels, we used RNA interference (RNAi) to evaluate the effect of depleting endogenous WNK4 on NCC protein expression. Because other investigators have reported RNAi-mediated knock down of WNK4 mRNA in human embryonic kidney cells (20), we screened HEK 293H cells for endogenous WNK4 protein. Using an established anti-human WNK4 antibody (27, 28), we detected a single band at the predicted molecular weight of full-length human WNK4 (135 kDa) (Fig. 5*B*). For the RNAi experiments, 293H cells stably expressing moderate levels of 2×HA-NCC were transfected with siRNAs against WNK4 or a scrambled siRNA control. 24 h after transfection, cells were lysed, and total 2×HA-NCC protein abundance was assessed by anti-HA dot-blotting. In two separate studies utilizing siRNA duplexes targeted to different regions of the human WNK4 mRNA sequence, we found that the depletion of endogenous WNK4 protein levels by greater than 60% resulted in a statistically significant increase in total NCC protein abundance of ~20% (Fig. 5*B*). These findings therefore confirm that WNK4 reduces the steady state protein abundance of NCC and establish that this effect takes place when the kinase is present at its usual expression levels.

The observation that WNK4 inhibits NCC forward trafficking and decreases NCC steady state protein abundance suggests that the kinase might route NCC away from the plasma membrane and to a degradative intracellular organelle, such as the lysosome or the proteasome. To evaluate these pathways of degradation, we measured the WNK4 effect on NCC protein abundance in the absence and presence of the selective lysosomal protease inhibitor leupeptin or the proteasome inhibitor MG-132. Coexpression of WNK4 with 2×HA-NCC resulted in a 45% reduction in total protein abundance, an effect that was significantly blocked by lysosomal protease inhibition ($p < 0.05$, Fig. 6*A*). Although an 18-h incubation with 5 μM MG-132 increased NCC total protein abundance compared with DMSO vehicle-treated cells (data not shown), proteasome inhibition did not significantly alter the reduction in NCC protein abundance seen with WNK4 coexpression (Fig. 6*A*). These data therefore indicate that the effect of WNK4 to reduce NCC protein abundance is specifically sensitive to inhibitors of the lysosome but not inhibitors of the proteasome.

To verify that the inhibitory effect of WNK4 on NCC surface expression was truly due to a change on NCC trafficking to the cell surface and not simply an artifact of decreased total protein abundance, we performed 2×HA-NCC surface expression measurements in the absence or presence of WNK4 in cells that were pretreated with lysosomal protease inhibitors, and normalized the surface expression data to total protein density. These studies revealed that despite leupeptin treatment and normalization of the surface expression measurements to total cellular protein, WNK4 still reduced the surface expression of the cotransporter by half (Fig. 6*B*). This finding indicates that WNK4 diverts NCC from the cell surface and that a substantial fraction of the total diverted cotransporter pool becomes

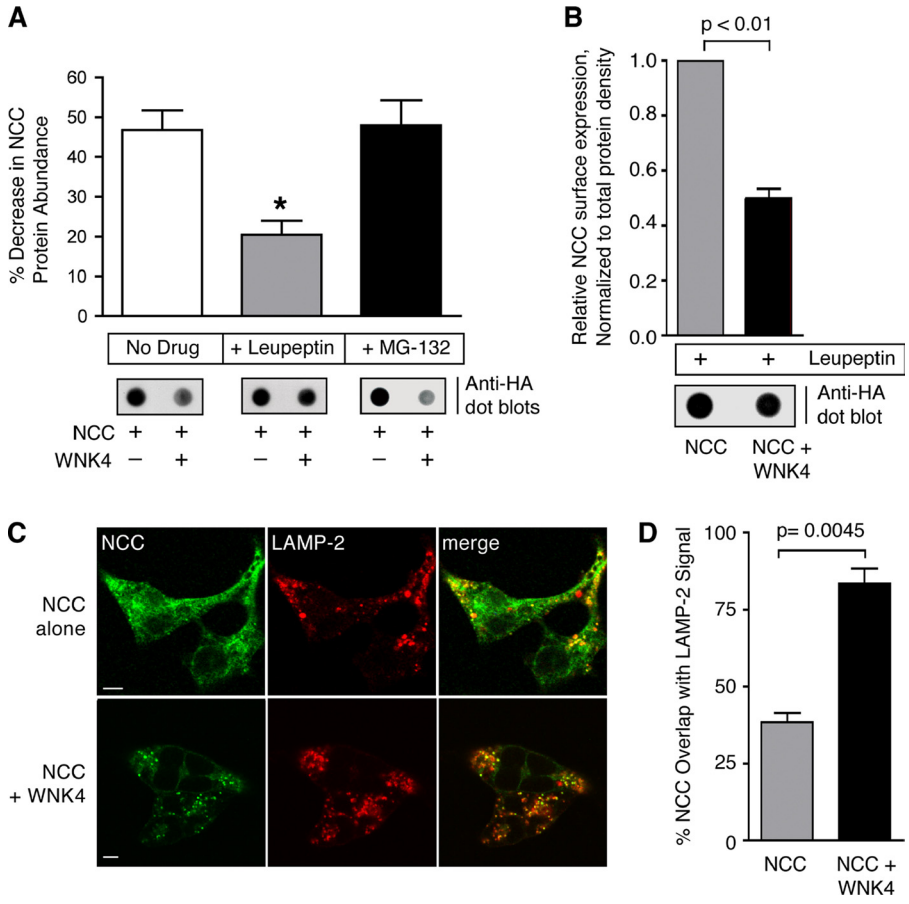

FIGURE 6. **WNK4 diverts NCC to the lysosomal pathway.** *A*, protein densitometry measurements of HEK-293H cells transiently expressing 2×HA-NCC plus empty vector or 2×HA-NCC plus WNK4, treated in the absence and presence of leupeptin (10 μM for 14 h) and MG-132 (5 μM for 18 h). Shown *below the bar graphs* are representative anti-HA dot blots of the whole cell lysates (7 μg). For the MG-132-treated samples, the exposure time of the blot was shortened to avoid oversaturation of the film and improve quantitative accuracy. In cells expressing NCC and WNK4, leupeptin but not MG-132 treatment significantly attenuated the reduction in total cotransporter protein density caused by WNK4 (mean ± S.E., $n = 4–6$ experiments). *, $p < 0.05$ by one-way analysis of variance, Dunnett's post-hoc test. *B*, cell surface luminometry measurements of cells transiently expressing NCC in the absence or presence of WNK4 treated with 10 μM leupeptin for 14 h. The cell surface expression measurements were normalized to the total NCC protein density of transfected and leupeptin-treated whole cell lysates prepared in parallel to the luminometry assays. A representative anti-HA dot blot of the protein densities (7 μg of whole cell lysate) is shown *below the bar graph* (mean ± S.E., $n = 4$). *C*, laser scanning confocal images of HEK-293H cells stably expressing 2×HA-NCC, transiently transfected with either empty vector or Myc-tagged WNK4, and treated with leupeptin for 14 h. HA-tagged NCC and endogenous LAMP-2 were labeled using Alexa Fluor 488- and 568-conjugated secondary antibodies, respectively. In samples transiently transfected with WNK4, cells expressing Myc epitopes were identified using Alexa Fluor 635 secondary antibodies (not shown). *Scale bar* = 10 μm. *D*, quantification of the degree of overlap between the 2×HA-NCC and LAMP-2 signals in the absence and presence of WNK4. Results are the mean ± S.E., $n = 20$ cells per group collected across three separate transfections.

retained within an intracellular compartment whose cargo is normally subject to degradation by lysosomal proteases.

To identify this intracellular compartment, we evaluated the subcellular localization of NCC in the absence or presence of WNK4 by immunofluorescence confocal microscopy. HEK-293H cells stably expressing 2×HA-NCC were transiently transfected with Myc-tagged WNK4 or empty vector. Before fixation, the cells were pretreated with leupeptin for 12 h so that the pool of cotransporters that would normally be degraded in lysosomes could be visualized and quantified. The cells were then processed for confocal microscopy. In the Myc-WNK4-transfected samples, cells expressing Myc epitopes were identified, and the degree of NCC overlap with the lysosomal marker LAMP-2 was quantified for individual cells. As shown in Fig. 6*C*, in mock-transfected cells a moderate amount of cotransporter was visualized in intracellular puncta that overlapped with the LAMP-2 signal. In contrast, the degree of NCC overlap with LAMP-2 increased substantially from 34 to 80% in cells that transiently expressed WNK4 ($p = 0.0045$, Figs. 6, *C* and *D*). These findings demonstrate that the coexpression of WNK4 with NCC promotes the accumulation of the cotransporter in lysosomes, verifying that WNK4 diverts NCC to the endolysosomal pathway for degradation.

WNK4 Stimulates a Physical Association between NCC and the AP-3 Complex—Our observations indicate that WNK4 suppresses NCC anterograde traffic to the cell surface while simultaneously enhancing its accumulation in lysosomes. Consequently, we reasoned that WNK4 might stimulate an interaction between NCC and trafficking machinery that directs cargo to lysosomes via an intracellular route. Analysis of the cytoplasmic domains of NCC revealed five canonical trafficking signals that could potentially interact with AP-3, a heterotetrameric adaptor that incorporates membrane proteins into vesicle carriers that target membrane proteins to lysosomes from sorting stations at endosomes or the TGN (29–33). As shown in Fig. 7*A*, all of the sequences conform to the canonical tyrosine-based motif Y*XX*ø, where X represents any amino acid, and ø represents a large bulky hydrophobic residue. Four of these putative sorting signals are contained within the NCC cytoplasmic carboxyl terminus, whereas one is harbored within the cotransporter amino terminus.

This observation prompted us to test whether NCC associates with AP-3 in a protein complex that is subject to regulation by WNK4. In these immunoprecipitation studies, HEK-293H cells stably expressing 2×HA-NCC were transiently transfected with empty vector or WNK4 and were pretreated with leupeptin to prevent the degradation of cotransporters in the lysosomal pathway. The cells were then lysed and immunoprecipitated with an antibody to the δ-adaptin subunit of the AP-3 complex. In the absence of exogenous WNK4, NCC immunoprecipitated to a modest degree with the δ-adaptin antibody (Fig. 7*B*). This signal increased substantially when NCC was

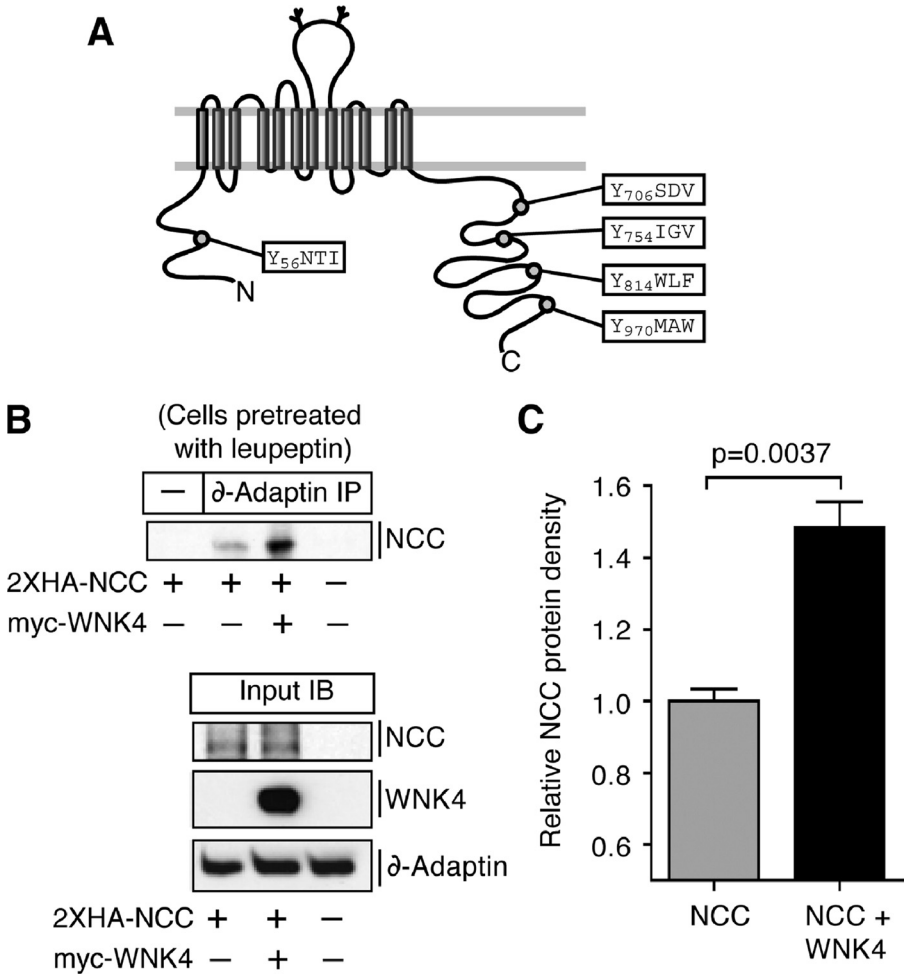

FIGURE 7. **WNK4 stimulates NCC interaction with endogenous AP-3 complexes.** *A*, schematic showing the location of five putative canonical AP-3 binding motifs embedded within the mouse NCC cytoplasmic domains. All of the identified sequences are tyrosine-based, are conserved in human NCC, and conform to the sequence Y*XX*ø. *B*, *top*, HEK-293H cells stably expressing 2×HA-NCC were transiently transfected with empty vector or Myc-WNK4, treated with leupeptin for 14 h before lysis. Whole cell lysates were subject to immunoprecipitation with anti-δ-adaptin antibody and immunoblotted with anti-HA antibody. *Bottom*, 3% of the whole cell lysate inputs for the immunoprecipitation (*IP*) were immunoblotted (*IB*) for 2×HA-NCC, Myc-WNK4, and endogenous δ-adaptin. *C*, quantification of the NCC signal in the δ-adaptin immunoprecipitates, measured by protein densitometry (mean ± S.E., $n = 3$).

coexpressed with the kinase. Quantification of multiple experiments demonstrated that WNK4 enhanced the amount of NCC that immunoprecipitated with the δ-adaptin antibody by 42% ($p = 0.0037$; Fig. 7*C*). In contrast, immunoprecipitation studies performed with an antibody directed to the α-adaptin subunit of the AP-2 complex, an adaptor that mediates clathrin dependent endocytosis of cargo from the plasma membrane, were unsuccessful at demonstrating an association between NCC and AP-2 above background (data not shown). These data demonstrate that a portion of the total cellular NCC pool interacts physically with AP-3 and that this fraction is increased in the presence of WNK4. Thus, these findings indicate a mechanism by which the kinase may promote NCC routing to the lysosome.

Overexpression of WNK4 Promotes an Increase in Total Lysosomal Content—In our analyses of subcellular NCC localization, it became evident that WNK4 may increase the total amount of LAMP-2-positive content per cell (note the differences in LAMP-2 staining in Fig. 6*C*). Thus, we considered that WNK4 might generally enhance AP-3-dependent lysosomal routing and/or promote lysosomal biogenesis. To address this question, we quantified the total LAMP-2 signal in 293H cells transiently transfected with either WNK4 or empty vector. In these experiments, cells were purposely studied without NCC to evaluate lysosomes independent of NCC routing. As shown in Fig. 8*A*, WNK4-transfected cells exhibited an increase in LAMP-2 staining. Quantification of the LAMP-2-positive signal per unit of cytoplasmic area revealed that the kinase increased the fractional content of the lysosomal marker from 6 to 12% ($p < 0.001$; Fig. 8*B*). These findings suggest the kinase may regulate NCC by a mechanism that involves a generalized up-regulation of the lysosomal routing pathway, such as through AP-3 activation.

DISCUSSION

In this study we have defined the mechanism by which WNK4 influences the intracellular trafficking of NCC. Using several approaches to monitor the plasma membrane trafficking of the cotransporter, we find that WNK4 selectively suppresses the rate of NCC delivery from the TGN to the plasma membrane without affecting its rate of internalization. In addition, WNK4 coexpression with NCC causes the cotransporter to be degraded via a leupeptin-sensitive pathway and increases the fraction of NCC that colocalizes with a lysosomal marker, LAMP-2. Last, we find that WNK4 enhances the physical association between NCC and AP-3, an adaptor responsible for directing cargo to the lysosome via an intracellular route. Taken together, these observations indicate that WNK4 decreases the efficiency of NCC cell surface delivery by diverting the cotransporter to the endolysosomal system for degradation.

The work presented here defines a novel mechanism that expands upon and unifies several disparate observations regarding WNK4-mediated NCC regulation. Golbang *et al.* (6) reported that the effect of WNK4 on NCC surface expression was insensitive to coexpression with dynamin K44A, a dominant negative dynamin mutant. In addition, they noted that in *Xenopus* oocytes expressing a high plasma membrane abundance of the cotransporter 3 days post-injection, 24 h of BFA treatment yielded no difference in the effect of WNK4 on NCC surface expression. Based on these findings, the authors speculated that WNK4 might not accelerate the dynamin-dependent

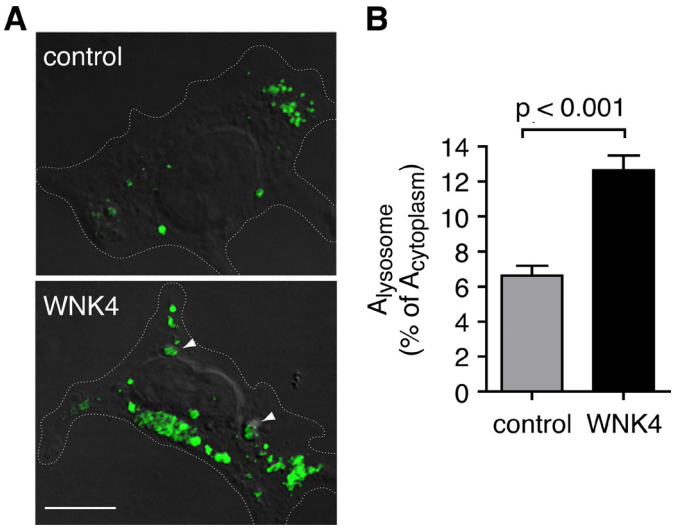

FIGURE 8. **WNK4 promotes a generalized increase in total lysosomal content.** *A*, laser-scanning confocal images of HEK-293H cells transiently transfected with either empty vector or Myc-tagged WNK4, pretreated with leupeptin for 14 h. Endogenous LAMP-2 was labeled using an Alexa Fluor 488-conjugated secondary antibodies. Cells expressing Myc epitopes were identified using an Alexa Fluor 568-conjugated secondary antibodies (not shown), and images of the LAMP-2 positive signal were superimposed over concurrently taken differential interference contrast images. Cell outlines are marked with a *dotted line*. Representative lysosomal structures are indicated with *arrowheads*. *Scale bar* = 10 μm. *B*, quantification of the total LAMP-2-positive signal per cell ($A_{lysosome}$) expressed as a percentage of total cytoplasmic area ($A_{cytoplasm}$) (mean ± S.E., n = 27–31 cells per experimental group, collected across three separate transfections).

endocytosis of the cotransporter. Here, our direct measurements of NCC trafficking demonstrate that this idea is in fact the case, as they show that WNK4 suppresses the plasma membrane delivery of NCC from the biosynthetic pathway and does not alter the cotransporter rate of endocytic trafficking. A different study of NCC and WNK4 by Cai *et al.* (7) found that the protein abundance of NCC was sensitive to bafilomycin-induced changes in endosomal pH. These data suggest that WNK4 augments NCC trafficking to a degradative pathway that involves endosomes. Our findings extend these observations, as they identify the compartment where NCC routing occurs and define a mechanism by which NCC arrives at that compartment. Specifically, the sensitivity of NCC to lysosomal protease inhibition, the direct visualization of the cotransporter in lysosomes, and the observation that WNK4 enhances an association between NCC and AP-3 provide strong evidence that the kinase enhances NCC lysosomal trafficking. Thus, the data presented here resolve previous gaps in our knowledge of WNK4-mediated NCC regulation, establishing that the kinase stimulates NCC trafficking via a known intracellular route that ultimately controls the cotransporter cell surface numbers.

AP-3 is one of a short list of known adaptors that modulate membrane protein transport to the lysosome. The ubiquitous AP-3 isoform interacts with lysosomal membrane proteins from endosomes and/or the TGN and marks those cargos for incorporation into vesicle carriers that eventually fuse with lysosomes. Cargo binding via the μ3 subunit requires the presence of a Y*XX*ø motif (31), whereas dileucine-based motifs conforming to the sequence (D/E)*XXX*L(L/I) mediate a more complex interaction that involves multiple AP-3 subunits (34). The relative positions of these canonical signals and the context of amino acid residues surrounding them play important roles in determining how they interact with the AP-3 and hence, the endosomal sorting machinery.

Our observations that NCC associates with the δ subunit of AP-3 and that WNK4 enhances this interaction provide evidence that the kinase may act as a switch that diverts the course of NCC traffic away from its functional destination at the cell surface to a pathway that leads to its lysosomal degradation. Although much of the literature on AP-3-mediated sorting has focused on its interactions with cargos that normally reside in lysosomes at steady state, there are some reported examples of membrane proteins expressed at the plasma membrane that are directed to the lysosome via an AP-3 dependent route. For example, the brain-specific water channel AQP4 contains a Y*XX*ø motif positioned close to a serine residue, which when phosphorylated stimulates μ3 binding, switching its transport to lysosomes for degradation (35). In our study we identified multiple Y*XX*ø motifs in the NCC sequence that could potentially bind to μ3 (Fig. 7*A*). Although it is likely that AP-3 directly recognizes one or more of these sequences, it is entirely possible that an intermediary protein maybe involved, as membrane proteins can be selected for lysosomal routing via indirect AP-3 interactions (36). Our observations that WNK4 also promotes LAMP-2 delivery to lysosomes raise the intriguing possibility that the kinase may switch NCC to an AP-3-dependent route by stimulating generalized AP-3 activity in the endolysosomal pathway. The details of this mechanism remain to be determined and serve as grounds for future investigation.

In the distal nephron, several WNKs, including WNK4, WNK1, KS-WNK1, and WNK3, participate in an aldosterone-regulated signaling network that coordinates sodium chloride reabsorption via NCC and potassium secretion via the potassium channel ROMK (13, 37–39). As was recently shown with NCC (40), the relative abundances and activation states of the components of the network precisely determines the transport characteristics of its regulatory targets over a very wide functional range. Thus, it has been hypothesized that the network may act as a "rheostat" which allows the distal nephron to fine-tune the electrolyte contents of the urine to meet the demands of extracellular fluid volume and potassium balance. Although it has been recognized that under certain physiological circumstances the renin-angiotensin-aldosterone system primarily functions to retain Na^+ and defend intravascular volume, whereas under other conditions it preferentially acts to promote kaluresis (41), the underlying mechanism by which one pathway could carry out such dissimilar effects has remained elusive. Coupled with recent observations regarding the effect of WNK4 on ROMK trafficking, our data may shed light on this divergent mechanism. A study by He *et al.* (42) showed that WNK4 and WNK1 regulate ROMK surface expression by stimulating its clathrin-dependent endocytosis in an intersectin-dependent manner. Moreover, recent studies by our group demonstrate that WNK-stimulated ROMK endocytosis requires the autosomal recessive hypercholesterolemia protein, a phosphotyrosine binding domain-containing clathrin coat-associated adaptor which couples ROMK selection to the endocytic machinery (43). In contrast to these findings for ROMK, the

data presented here demonstrate that WNK4 regulates NCC trafficking by an entirely different process, as it exerts no effect on cell surface lifetime and instead suppresses forward trafficking by diverting the cotransporter directly to the lysosome. Together, these findings indicate that WNKs are capable of influencing two distinct trafficking processes that regulate separate ion transport pathways. Accordingly, we propose that certain physiologic perturbations, such as a change in sodium balance or total body potassium content, may favor the regulation of one trafficking pathway over the other. Depending on the physiologic circumstance, WNK signaling in the distal nephron might modulate WNK4 function to affect the endocytosis of the potassium secretory machinery or, alternatively, influence the biosynthetic trafficking of NaCl cotransporters, leading to precise but diversified control of the final electrolyte composition of the urine.

In summary, we have provided evidence that WNK4 suppresses the forward trafficking and plasma membrane delivery of NCC, diverting the cotransporter to lysosomes via a sorting mechanism that involves AP-3. Thus, WNK4 influences the steady state cell surface expression of NCC by altering the balance between plasma membrane delivery and lysosomal degradation.

Acknowledgments—We thank Amanda K. Mason, Donghui Ma, Liang Fang, Bo-Young Kim, and Bernardo Ortega for helpful discussions and technical assistance.

REFERENCES

1. Kahle, K. T., Ring, A. M., and Lifton, R. P. (2008) *Annu. Rev. Physiol.* **70,** 329–355
2. Yang, C. L., Angell, J., Mitchell, R., and Ellison, D. H. (2003) *J. Clin. Invest.* **111,** 1039–1045
3. Kahle, K. T., Wilson, F. H., Leng, Q., Lalioti, M. D., O'Connell, A. D., Dong, K., Rapson, A. K., MacGregor, G. G., Giebisch, G., Hebert, S. C., and Lifton, R. P. (2003) *Nat. Genet.* **35,** 372–376
4. Wilson, F. H., Disse-Nicodème, S., Choate, K. A., Ishikawa, K., Nelson-Williams, C., Desitter, I., Gunel, M., Milford, D. V., Lipkin, G. W., Achard, J. M., Feely, M. P., Dussol, B., Berland, Y., Unwin, R. J., Mayan, H., Simon, D. B., Farfel, Z., Jeunemaitre, X., and Lifton, R. P. (2001) *Science* **293,** 1107–1112
5. Wilson, F. H., Kahle, K. T., Sabath, E., Lalioti, M. D., Rapson, A. K., Hoover, R. S., Hebert, S. C., Gamba, G., and Lifton, R. P. (2003) *Proc. Natl. Acad. Sci. U.S.A.* **100,** 680–684
6. Golbang, A. P., Cope, G., Hamad, A., Murthy, M., Liu, C. H., Cuthbert, A. W., and O'Shaughnessy, K. M. (2006) *Am. J. Physiol. Renal Physiol.* **291,** F1369–1376
7. Cai, H., Cebotaru, V., Wang, Y. H., Zhang, X. M., Cebotaru, L., Guggino, S. E., and Guggino, W. B. (2006) *Kidney Int.* **69,** 2162–2170
8. Yang, S. S., Yamauchi, K., Rai, T., Hiyama, A., Sohara, E., Suzuki, T., Itoh, T., Suda, S., Sasaki, S., and Uchida, S. (2005) *Biochem. Biophys. Res. Commun.* **330,** 410–414
9. Lalioti, M. D., Zhang, J., Volkman, H. M., Kahle, K. T., Hoffmann, K. E., Toka, H. R., Nelson-Williams, C., Ellison, D. H., Flavell, R., Booth, C. J., Lu, Y., Geller, D. S., and Lifton, R. P. (2006) *Nat. Genet.* **38,** 1124–1132
10. Yang, S. S., Morimoto, T., Rai, T., Chiga, M., Sohara, E., Ohno, M., Uchida, K., Lin, S. H., Moriguchi, T., Shibuya, H., Kondo, Y., Sasaki, S., and Uchida, S. (2007) *Cell Metab.* **5,** 331–344
11. Kunchaparty, S., Palcso, M., Berkman, J., Velázquez, H., Desir, G. V., Bernstein, P., Reilly, R. F., and Ellison, D. H. (1999) *Am. J. Physiol.* **277,** F643–649
12. Yang, C. L., Zhu, X., Wang, Z., Subramanya, A. R., and Ellison, D. H. (2005) *J. Clin. Invest.* **115,** 1379–1387
13. Subramanya, A. R., Yang, C. L., Zhu, X., and Ellison, D. H. (2006) *Am. J. Physiol. Renal Physiol.* **290,** F619–624
14. Bostanjoglo, M., Reeves, W. B., Reilly, R. F., Velázquez, H., Robertson, N., Litwack, G., Morsing, P., Dørup, J., Bachmann, S., and Ellison, D. H. (1998) *J. Am. Soc. Nephrol.* **9,** 1347–1358
15. Ma, D., Tang, X. D., Rogers, T. B., and Welling, P. A. (2007) *J. Biol. Chem.* **282,** 5781–5789
16. Yoo, D., Fang, L., Mason, A., Kim, B. Y., and Welling, P. A. (2005) *J. Biol. Chem.* **280,** 35281–35289
17. Mason, A. K., Jacobs, B. E., and Welling, P. A. (2008) *J. Biol. Chem.* **283,** 5973–5984
18. Griffiths, G., Pfeiffer, S., Simons, K., and Matlin, K. (1985) *J. Cell Biol.* **101,** 949–964
19. Ladinsky, M. S., Wu, C. C., McIntosh, S., McIntosh, J. R., and Howell, K. E. (2002) *Mol. Biol. Cell* **13,** 2810–2825
20. Lazrak, A., Liu, Z., and Huang, C. L. (2006) *Proc. Natl. Acad. Sci. U.S.A.* **103,** 1615–1620
21. Pelham, H. R. (1991) *Cell* **67,** 449–451
22. Shimkets, R. A., Lifton, R. P., and Canessa, C. M. (1997) *J. Biol. Chem.* **272,** 25537–25541
23. Schwake, M., Friedrich, T., and Jentsch, T. J. (2001) *J. Biol. Chem.* **276,** 12049–12054
24. Peng, Y., Amemiya, M., Yang, X., Fan, L., Moe, O. W., Yin, H., Preisig, P. A., Yanagisawa, M., and Alpern, R. J. (2001) *Am. J. Physiol. Renal Physiol.* **280,** F34–42
25. Lee-Kwon, W., Kawano, K., Choi, J. W., Kim, J. H., and Donowitz, M. (2003) *J. Biol. Chem.* **278,** 16494–16501
26. Pfeiffer, S., Fuller, S. D., and Simons, K. (1985) *J. Cell Biol.* **101,** 470–476
27. Song, J., Hu, X., Riazi, S., Tiwari, S., Wade, J. B., and Ecelbarger, C. A. (2006) *Am. J. Physiol. Renal Physiol.* **290,** F1055–1064
28. Kahle, K. T., Gimenez, I., Hassan, H., Wilson, F. H., Wong, R. D., Forbush, B., Aronson, P. S., and Lifton, R. P. (2004) *Proc. Natl. Acad. Sci. U.S.A.* **101,** 2064–2069
29. Simpson, F., Peden, A. A., Christopoulou, L., and Robinson, M. S. (1997) *J. Cell Biol.* **137,** 835–845
30. Peden, A. A., Oorschot, V., Hesser, B. A., Austin, C. D., Scheller, R. H., and Klumperman, J. (2004) *J. Cell Biol.* **164,** 1065–1076
31. Dell'Angelica, E. C., Ohno, H., Ooi, C. E., Rabinovich, E., Roche, K. W., and Bonifacino, J. S. (1997) *EMBO J.* **16,** 917–928
32. Boehm, M., and Bonifacino, J. S. (2002) *Gene* **286,** 175–186
33. Newell-Litwa, K., Seong, E., Burmeister, M., and Faundez, V. (2007) *J. Cell Sci.* **120,** 531–541
34. Janvier, K., Kato, Y., Boehm, M., Rose, J. R., Martina, J. A., Kim, B. Y., Venkatesan, S., and Bonifacino, J. S. (2003) *J. Cell Biol.* **163,** 1281–1290
35. Madrid, R., Le Maout, S., Barrault, M. B., Janvier, K., Benichou, S., and Mérot, J. (2001) *EMBO J.* **20,** 7008–7021
36. Duffield, A., Kamsteeg, E. J., Brown, A. N., Pagel, P., and Caplan, M. J. (2003) *Proc. Natl. Acad. Sci. U.S.A.* **100,** 15560–15565
37. Wade, J. B., Fang, L., Liu, J., Li, D., Yang, C. L., Subramanya, A. R., Maouyo, D., Mason, A., Ellison, D. H., and Welling, P. A. (2006) *Proc. Natl. Acad. Sci. U.S.A.* **103,** 8558–8563
38. McCormick, J. A., Yang, C. L., and Ellison, D. H. (2008) *Hypertension* **51,** 588–596
39. O'Reilly, M., Marshall, E., Macgillivray, T., Mittal, M., Xue, W., Kenyon, C. J., and Brown, R. W. (2006) *J. Am. Soc. Nephrol.* **17,** 2402–2413
40. Yang, C. L., Zhu, X., and Ellison, D. H. (2007) *J. Clin. Invest.* **117,** 3403–3411
41. Halperin, M. L., and Kamel, K. S. (2000) *Can. J. Physiol. Pharmacol.* **78,** 587–594
42. He, G., Wang, H. R., Huang, S. K., and Huang, C. L. (2007) *J. Clin. Invest.* **117,** 1078–1087
43. Fang, L., Kim, B. Y., Wade, J. B., and Welling, P. A. (2008) *FASEB J.* **22,** 1158.9